Causes, consequences, and remedies for growth-induced solid stress in murine and human tumors

Triantafyllos Stylianopoulos[a,b,1], John D. Martin[a,c,1], Vikash P. Chauhan[a,d], Saloni R. Jain[a,c], Benjamin Diop-Frimpong[a,d,e], Nabeel Bardeesy[f], Barbara L. Smith[g], Cristina R. Ferrone[h], Francis J. Hornicek[i], Yves Boucher[a], Lance L. Munn[a], and Rakesh K. Jain[a,2]

[a]Edwin L. Steele Laboratory, Department of Radiation Oncology, Massachusetts General Hospital and Harvard Medical School, Boston, MA 02114; [b]Department of Mechanical and Manufacturing Engineering, University of Cyprus, 1678 Nicosia, Cyprus; [c]Department of Chemical Engineering, Massachusetts Institute of Technology, Cambridge, MA 02139; [d]Harvard School of Engineering and Applied Sciences, Harvard University, Cambridge, MA 02138; [e]Harvard–MIT Division of Health Sciences and Technology, Cambridge, MA 02138; [f]Cancer Center and Center for Regenerative Medicine, Massachusetts General Hospital and Harvard Medical School, Boston, MA 02114; [g]Department of Surgery, Gillette Center for Women's Cancers, Massachusetts General Hospital and Harvard Medical School, Boston, MA 02114; [h]Department of Surgery, Pancreas and Biliary Surgery Program, Massachusetts General Hospital and Harvard Medical School, Boston, MA 02114; and [i]Orthopedic Oncology Service, Center for Sarcoma and Connective Tissue Oncology, Massachusetts General Hospital and Harvard Medical School, Boston, MA 02114

This contribution is part of the special series of Inaugural Articles by members of the National Academy of Sciences elected in 2009.

Contributed by Rakesh K. Jain, August 2, 2012 (sent for review December 5, 2011)

The presence of growth-induced solid stresses in tumors has been suspected for some time, but these stresses were largely estimated using mathematical models. Solid stresses can deform the surrounding tissues and compress intratumoral lymphatic and blood vessels. Compression of lymphatic vessels elevates interstitial fluid pressure, whereas compression of blood vessels reduces blood flow. Reduced blood flow, in turn, leads to hypoxia, which promotes tumor progression, immunosuppression, inflammation, invasion, and metastasis and lowers the efficacy of chemo-, radio-, and immunotherapies. Thus, strategies designed to alleviate solid stress have the potential to improve cancer treatment. However, a lack of methods for measuring solid stress has hindered the development of solid stress-alleviating drugs. Here, we present a simple technique to estimate the growth-induced solid stress accumulated within animal and human tumors, and we show that this stress can be reduced by depleting cancer cells, fibroblasts, collagen, and/or hyaluronan, resulting in improved tumor perfusion. Furthermore, we show that therapeutic depletion of carcinoma-associated fibroblasts with an inhibitor of the sonic hedgehog pathway reduces solid stress, decompresses blood and lymphatic vessels, and increases perfusion. In addition to providing insights into the mechanopathology of tumors, our approach can serve as a rapid screen for stress-reducing and perfusion-enhancing drugs.

tumor microenvironment | desmoplastic tumors | pancreatic ductal adenocarcinoma | mathematical modeling | sonic hedgehog pathway

Elevated interstitial fluid pressure (IFP) and solid stress are hallmarks of the mechanical microenvironment of solid tumors (1). IFP is the isotropic stress (i.e., applied equally in all directions) exerted by the fluid, whereas solid stress is exerted by the nonfluid components. In 1950, the work by Young et al. (2) provided the first measurements of IFP in tumors growing in rabbits and found it to be elevated compared with IFP in normal testicular tissue. However, the implications of this interstitial hypertension for tumor progression and treatment were not fully revealed for nearly four decades. In 1988, we developed a mathematical model that showed that IFP is uniformly elevated throughout the bulk of a tumor and precipitously drops to normal values in the tumor margin, causing a steep pressure gradient (3, 4). Based on the model's results, we predicted that diffusion rather than convection would be the dominant mode of transport within tumors because of nearly uniform pressure within the tumor. Furthermore, we predicted that the steep pressure gradients in the periphery would cause fluid leaking from the blood vessels located in the tumor margin—but not from the vessels in the tumor interior—to ooze into the surrounding normal tissue. This oozing fluid would facilitate transport of growth factors and cancer cells into the surrounding tissue—fueling tumor growth, progression, and lymphatic metastasis. In subsequent years, we confirmed these predictions about IFP experimentally in both animal models and human tumors (5–15). Moreover, we revealed the key mechanisms leading to the elevated IFP—high vascular permeability coupled with mechanical compression of downstream blood vessels and draining lymphatic vessels (16–18). We also posited that the high vascular permeability would cause flow stasis in tumor vessels, further compromising drug delivery (19, 20).

Realizing the adverse consequences of abnormal function of tumor vessels, we proposed that the judicious application of antiangiogenic agents would normalize tumor vessels and improve their function. Specifically, the decreased vascular permeability would decrease IFP and increase blood flow in previously static blood vessels, thereby increasing drug delivery and treatment efficacy of a number of therapies (1, 21, 22). We and others have provided compelling evidence in support of this therapeutic strategy in both animal and human tumors (14, 22–27). More crucially, we have shown that the extent of vascular normalization and the resulting increase in tumor blood perfusion correlate with increased survival of brain tumor patients receiving antiangiogenic therapy (28, 29). Understanding the causes and consequences of vessel leakiness and elevated IFP enabled us to find a clinically translatable strategy to improve the treatment outcome (22). However, vascular normalization by antiangiogenic agents can only improve the function of vessels that have an open lumen and are not compressed by solid stress. Thus, a better understanding of the solid stress present in tumors is needed to develop new therapies and further improve treatment outcome.

In contrast to the elevated IFP, much less is known about the causes, consequences, and remedies for solid stresses in tumors. It is assumed that solid stress is accumulated within tumors,

Author contributions: T.S., J.D.M., V.P.C., and R.K.J. designed research; T.S., J.D.M., V.P.C., S.R.J., and B.D.-F. performed research; N.B., B.L.S., C.R.F., and F.J.H. contributed new reagents/analytic tools; T.S., J.D.M., V.P.C., Y.B., L.L.M., and R.K.J. analyzed data; and T.S., J.D.M., L.L.M., and R.K.J. wrote the paper.

Conflict of interest statement: R.K.J. received research grants from Dyax, MedImmune, and Roche; received consultant fees from Dyax, Enlight, Noxxon, and SynDevRx; owns equity in Enlight, SynDevRx, and XTuit; and serves on the Board of Directors of XTuit and Board of Trustees of H&Q Healthcare Investors and H&Q Life Sciences Investors. No reagents or funding from these companies were used in these studies. Therefore, there is no significant financial or other competing interest in the work.

Freely available online through the PNAS open access option.

[1]T.S. and J.D.M. contributed equally to this work.

[2]To whom correspondence should be addressed. E-mail: jain@steele.mgh.harvard.edu.

This article contains supporting information online at www.pnas.org/lookup/suppl/doi:10.1073/pnas.1213353109/-/DCSupplemental.

because the proliferating cancer cells strain nearby structural elements of tumor and normal tissues. Some of the stress within the tumor is contributed by reciprocal forces from the surrounding normal tissue; the rest is stored within cells and matrix components of the tumor, and thus, it persists after the tumor is excised and external loads are removed. This stored stress is referred to as growth-induced solid or residual stress (30). By compressing blood and lymphatic vessels and creating hypoxia and interstitial hypertension, these solid stresses contribute to tumor progression and resistance to various treatments (1).

Because there were no simple techniques available to measure solid stresses in tumors in vivo, initially, we relied on in vitro studies and mathematical models. In 1997, we provided estimates of the magnitude of solid stresses in tumor spheroids, which represent an avascular phase of a tumor (31). We found that an external stress applied to a tumor spheroid inhibits tumor growth by decreasing proliferation and increasing apoptosis. In addition, the external stress field determines the shape of the spheroid. Using material properties of tumor tissue measured independently, we estimated the maximum magnitude of the solid stress to be in the range of 45–120 mmHg (6–16 kPa). In 2009, we provided a more accurate measurement of the growth-induced stress and found it to be 28 mmHg (3.7 kPa) (32). More recently, we have shown that the mechanical stress can also directly increase cancer cell invasion, aiding tumor progression (33).

Given the importance of solid stresses in tumor progression and treatment and lack of any in vivo data, we developed a mathematical model for solid stress based on our previous model for IFP. The model predicted a uniform compressive circumferential stress at the center of the tumor and tensile circumferential stress at the periphery (34). Moreover, the magnitude of the calculated compressive stress—comparable with the magnitude measured in spheroids (31, 32)—was large enough to compress vessels and nearby organs, obstruct large blood vessels with life-threatening consequences, or induce pain by pressing on nerves (18). By performing in vivo experiments, we confirmed that cancer cells could compress and collapse their own blood and lymphatic vessels, and destroying cancer cells around vessels could, indeed, reopen them (17, 18). However, whether other components of solid tumors contribute to the compressive stresses and how these components can be alleviated were not understood.

To this end, we develop a technique here to measure growth-induced solid stress in freshly excised human and animal tumors and investigate the effects of this stress on blood and lymphatic vessels. This technique involves measuring the extent of tissue relaxation after removing all external stresses and using these data to calculate the growth-induced solid stress with a mathematical model. We use this simple technique to show that solid stress is elevated in a range of murine and human tumors. Then, we use our technique to identify key components of tumors—cancer cells, stromal cells, collagen, and hyaluronan—that contribute to the generation and accumulation of growth-induced solid stress in tumors. Finally, we show that therapeutic depletion of carcinoma-associated fibroblasts (CAFs) with an inhibitor of the sonic hedgehog pathway reduces solid stress, decompresses vessels, and increases perfusion.

Results

Mathematical Modeling Guides Development of Our Experimental Technique. Growth-induced solid stress is extensively characterized in arterial, cardiac, and brain tissues (35–37). These tissues can be excised in such a way to retain growth-induced stress; a subsequent cut of the excised tissue then releases the stress, and the tissue deforms in a measurable way. Using the material properties characterizing tissue stiffness, mathematical models can be used to calculate the stress from the measured deformations. We hypothesized that tumor growth must strain solid components within the tumor, storing growth-induced stress. This stress is distinct from the solid stress that might be exerted on the tumor by the resistance of the confining normal tissue to the expansion of the tumor.

Acknowledging that tumors might be more fragile than these normal tissues, we set out to find the best way to make similar cuts to measure deformation and estimate growth-induced stresses in excised tumors. Using a computational model (details in *SI Materials and Methods*), we explored various modes of cutting and predicted the resulting deformations (Fig. 1). Cutting spheroids into hemispheres resulted in perpendicular swelling that was too small to measure in a clinical setting (Fig. 1*A*). Making a cut through an excised slab of tumor tissue produced measurable deformations (Fig. 1*B*). However, this proved inconsistent in practice, because the process of excising the slab often released the growth-induced stress before the final cut could be made. In another simulation, the model predicted that a partial cut through the center of the tumor (80% of the diameter) would result in a measurable deformation (Fig. 1*C*). The mode of deformation involves simultaneous swelling at the center and retraction at the boundary. These deformations arise from the model's assumption of compressive radial and circumferential stress in the center balanced by tensile circumferential stress at the boundary (34, 38) (Fig. 1 *D* and *E*). The release of this stress results in a significant

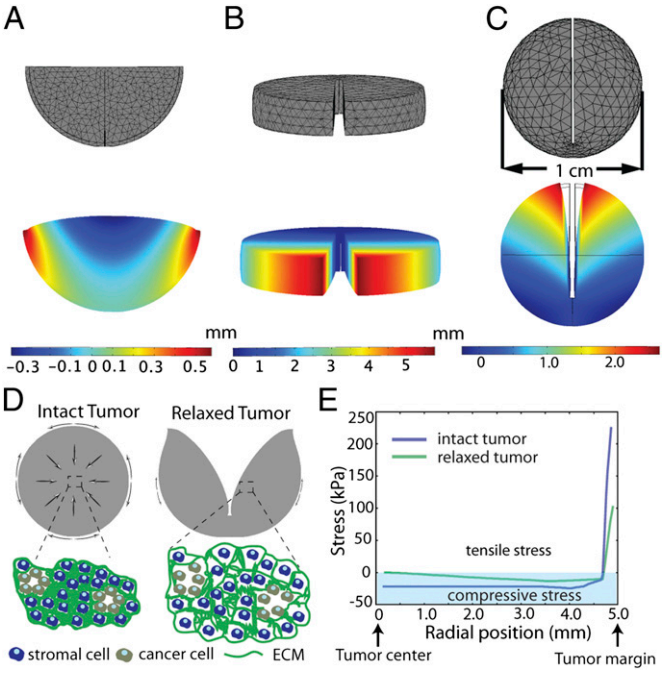

Fig. 1. Model predictions for the total displacement of the tumor after releasing the growth-induced stress by (*A*) cutting the tumor in one-half, (*B*) cutting a slice of the tumor, and (*C*) cutting the whole tumor. The tumor has a diameter of 1 cm, and the depth of the cut (*B* and *C*) is 0.8 cm. Notice the different displacement scales on the legends. Negative total displacements denote swelling (compressive stress), and positive total displacements denote opening (tensile stress) of the tissue. (*D*) Schematic of growth-induced stresses in tumors. In the tumor center, circumferential and radial stresses are compressive; in the periphery, radial stress is compressive, and circumferential stress is tensile (direction indicated with arrows). A partial cut through the center of the tumor (80% through the diameter) releases the stresses, and the tumor deforms in a measurable way. Compressive stresses in the tumor interior squeeze tumor components. After the tumor is cut and the stresses are released, the tumor interior decompresses (swells). (*E*) Spatial distribution of the circumferential growth-induced stress in an intact tumor and a tumor after making a cut. Compressive circumferential stresses at the tumor interior diminish, whereas tensile circumferential stresses at the periphery are also alleviated considerably.

gap or an opening at the location of the cut. Rigorous sensitivity analysis of the model (Figs. S1, S2, S3, S4, S5, and S6) confirmed that this approach was robust.

Estimation of Growth-Induced Stress in Transplanted and Human Tumors. To show that elevated growth-induced stress is a hallmark of solid tumors, we estimated growth-induced stress levels in tumors formed from nine different cancer cell lines implanted orthotopically in mice. We cut the tumors and measured the stress relaxation as the extent of tumor opening normalized to the diameter of the tumor (Fig. 2 *A*–*C*, Fig. S7, and Movie S1). Additional cuts of the relaxed halves did not result in appreciable shape changes. The experimental deformations confirmed the main assumptions of the model—stress in the tumor interior is compressive, and it is balanced by tensile circumferential stress at the periphery (Fig. 1*E*).

Calculation of growth-induced stress requires not only the extent of relaxation (normalized opening) but also the material properties of the tissue that characterize its stiffness. Thus, quantitative assessment of growth-induced stress requires material properties of each tumor analyzed. To calculate growth-induced stress, the experimentally measured tumor openings (Fig. 2*C*) were combined with previously measured or estimated material properties of tumor tissue (Table S1) and our mathematical model (details in *SI Materials and Methods*). From the material properties presented in Table S1, the stiffness is related to the shear modulus μ. Note that, although the U87 tumor exhibits similar extent of relaxation to the other tumor types (Fig. 2*C* and Fig. S7), it has much higher stress, because it is considerably stiffer than the other three tumors with stiffness that we measured previously (Tables S1 and S2). It is possible that other tumors may be stiffer than these tumors. Model predictions established that the compressive growth-induced stress in the interior of murine tumors ranged from 2.8 to 60.1 mmHg (0.37–8.01 kPa) (Table S2). This finding is consistent with previous estimates of compressive stress in multicellular tumor spheroids in vitro, which fall in the range of 28–120 mmHg (3.7–16.0 kPa) (31, 32).

Interestingly, the tumors with the highest stress exhibit the slowest growth rate (Table S2). Additionally, the extent of relaxation increased linearly with tumor volume before reaching a plateau, but it did not correlate with tumor density (mass per unit volume), which remained constant as volume increased (Fig. S8). These results show that growth-induced stress accumulates with growth and that this stress is independent of tumor density. Using the same procedure, we confirmed that the kidneys (Movie S2) of mice did not open measurably. These results support our hypothesis that growth-induced stress is elevated in tumors compared with normal noncontractile organs.

After validating the existence of growth-induced solid stress in murine tumors, we tested whether growth-induced stress was similarly elevated in human specimens. We performed tumor relaxation measurements in 10 malignant, freshly excised human

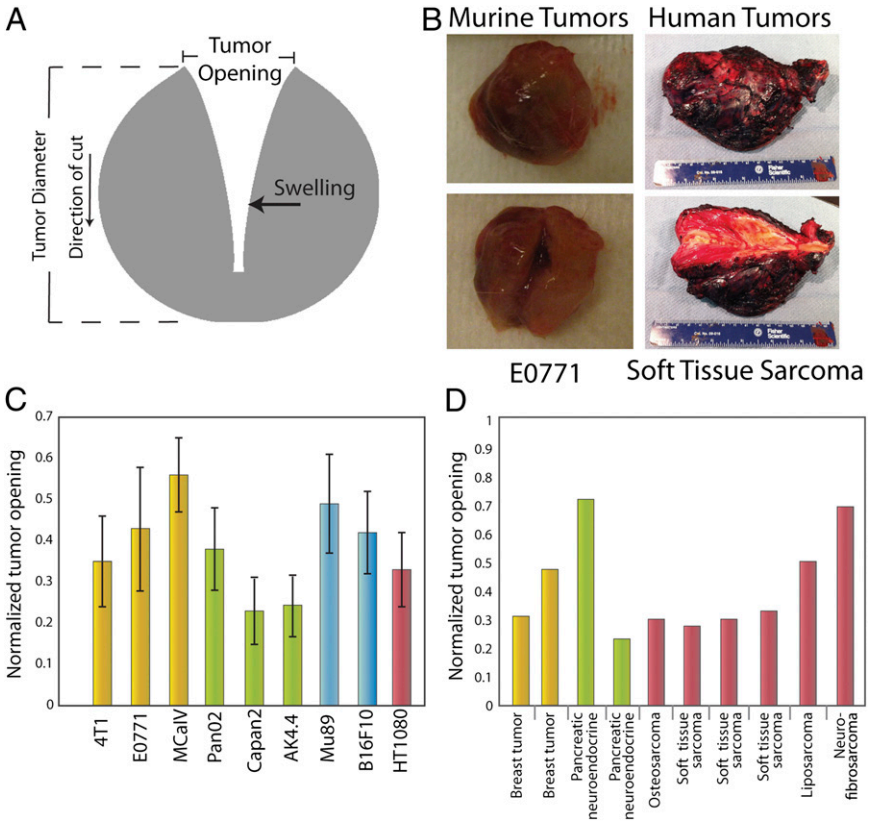

Fig. 2. Estimation of stress in transplanted and human tumors. (*A*) Schematic of tumor deformation after making a cut and releasing growth-induced stress. The retraction of the tumor at the surface is indicative of circumferential tension at the tumor margin, whereas the swelling of the inner surface at the point of cut is indicative of compression in the intratumoral region, which presumably balances the tension at the margin. Measuring the displacement (tumor opening) accounts for both retraction and swelling. (*B*) Photographs of the initial and final shape of tumors after making a cut. (*C* and *D*) Tumor openings were measured in transplanted orthotopic tumors surgically excised from mice and human tumors surgically excised from patients. The diameters of the mouse tumors (*C*) were ~1 cm, and the dimensions of the human tumors (*D*) are given in Table S3. Normalized tumor opening is the tumor opening as a fraction of the initial tumor diameter. For nonspherical tumors, an equivalent diameter was used for a sphere that has the same volume as the volume of the tumors. Yellow columns represent breast tumors, green columns represent pancreatic tumors, blue columns represent melanomas, and maroon columns represent sarcomas.

tumors. All deformed similarly to the transplanted murine tumors (Fig. 2 *B* and *D* and Fig. S9). Assuming a conservative estimate for the material properties of the human tumors (i.e., to provide upper bounds for the stresses), the calculated stresses ranged from 16.4 to 142.4 mmHg (2.2–19.0 kPa) (Table S3). Therefore, human tumors accumulate growth-induced stress similar to the tumors in our mouse models. After confirming that growth-induced solid stress is a general feature of solid tumors, we sought to identify tumor components that contribute to the generation and accumulation of stress.

Solid Stress Is Not Affected by IFP. Collapsed lymphatic and blood vessels are known to contribute to elevated IFP in tumors and not the other way around (9, 17, 18, 31). Therefore, we hypothesized that solid stress would not be affected by IFP. To this end, we developed a methodology that measures solid stress independent of fluid pressure. Other techniques, such as piezoelectric probes (39), measure a combination of solid stress and fluid pressure, making interpretation of results difficult. Indeed, measurements in the normal pancreas in situ using a piezoelectric probe were significantly higher than those measurements obtained by the wick-in-needle technique—an established technique to measure IFP (Table S4). Furthermore, the piezoelectric probe reported higher values in the pancreas in situ vs. exteriorized pancreas, suggesting that stress from the surrounding organs in the abdomen contributes to these measurements. Using the wick-in-needle technique, we also confirmed that growth-induced solid stress, which is solely contained within and transmitted by solid structural components, is not affected by the IFP (Fig. S10).

Cancer and Stromal Cells Generate Growth-Induced Solid Stress. Because cancer cells are known to compress vessels (17, 18), we hypothesized that they contribute to the accumulation of growth-induced stress. Proliferating cancer cells exert force on other cells and surrounding structures; the force on nearby components causes them to deform, resulting in accumulation of solid stress.

Because depletion of cancer cells likely changes the material properties in addition to stresses, determination of growth-induced stress levels before and after depletion requires knowledge of the corresponding material properties. However, our original goal was to develop an easy to implement and simple method to determine whether stress levels change after a stress-alleviating intervention. We recognized that, if two tumors shared the same stress level, a stiffer tumor would have less relaxation than a compliant one. Thus, after depletion of cancer cells, if compliant (i.e., treated) tumors open less than the more stiff control tumors, then we can conclude that cancer cell depletion reduces stress. The same principle applies to any other intervention that results in a reduction of stiffness.

To test this hypothesis, we depleted cancer cells and measured relaxation. In mice with orthotopic (human melanoma Mu89) or ectopic (human glioma U87) tumors (Fig. 3*A* and Fig. S11), we injected diphtheria toxin i.v. 24 h before tumor excision. We have shown previously that this treatment kills only human cells (18). Depletion of cancer cells in Mu89 and U87 tumors reduced the tumor opening by 40% and 30%, respectively ($P = 0.001$ for Mu89, $P = 0.026$ for U87; Student t test). These results show that cancer cells contribute to the generation of growth-induced stress.

Stromal cells, because they proliferate and contract to remodel the ECM (40), also apply forces on other tumor components. We, therefore, hypothesized that depleting fibroblasts would reduce growth-induced solid stress. To test this hypothesis, we coimplanted human breast CAFs with murine mammary adenocarcinoma cells in the mammary fat pad of female SCID mice using a method developed previously (41). To kill the human CAFs, we injected mice with diphtheria toxin. Tumors in which the CAFs were depleted had reduced relaxation and less human vimentin staining—a marker used to identify human CAFs (Fig. 3 *A* and *B* and Fig. S12). Because CAFs contribute to accumulation of growth-induced stress like cancer cells, we hypothesized that they compress vessels similar to the way that cancer cells compress vessels (17, 18). Indeed, we found that CAF-depleted tumors had larger mean vessel diameters (Fig. 3*C*), suggesting that depleting CAFs can improve perfusion in desmoplastic tumors.

ECM Contributes to Growth-Induced Solid Stress. Another prime candidate for accumulation of growth-induced stress is the ECM, which is composed of collagen, proteoglycans, and glycosaminoglycans (42–44). We hypothesized that collagen fibers contribute to growth-induced stress by virtue of the ability of these fibers to resist stretching, thereby confining the proliferating cells. Collagen fibers are also remodeled and pulled by fibroblasts (40, 45). Collagen resists tensile stress, because it becomes stiffer as it is stretched. This finding is true for both capsular (if present) and interstitial collagen, because the ECM in tumors is extensively cross-linked. Because our model and experiments have shown that tumors are in tension in the periphery and compression in the interior, we expect that peripheral collagen stores more stress than interior collagen. To assess the role of collagen in stress accumulation, we incubated the excised tumors in collagenase or serum (control arm) long enough for the enzymes to radially diffuse one-sixth of the tumors' radii and measured stress levels. We found that the tumor opening decreased

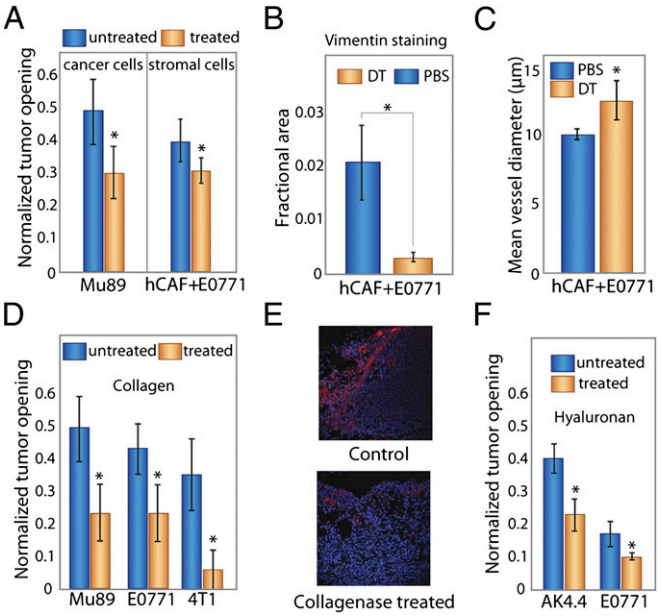

Fig. 3. Selective depletion of tumor constituents reduces growth-induced stress and decreases tumor opening. (*A*) Depletion with diphtheria toxin of human cancer cells in human Mu89 tumors or human stromal cells in E0771 tumors coimplanted with human CAFs decreased tumor opening ($P = 0.001$ and $P = 0.023$, respectively; Student t test). (*B*) Staining of E0771 tumors for colocalization of vimentin confirms that human fibroblast levels were reduced by diphtheria toxin treatment. The decrease in vimentin-stained area is significant ($P = 0.03$; Student t test). (*C*) Depletion of stromal cells also increased mean blood vessel diameter ($P = 0.05$; Student t test). (*D*) Treatment with bacterial collagenase decreased the tumor opening significantly and thus, the growth-induced stress for all tumors ($P = 0.003$ for Mu89, $P = 0.025$ for E0771, $P = 4 \times 10^{-6}$ for 4T1; Student t test). (*E*) Staining of Mu89 tumors for cell nuclei (blue) and collagen (red) shows reduction of collagen after treatment with collagenase. (*F*) Treatment with hyaluronidase also significantly decreased the tumor opening in AK4.4 and E0771 tumors ($P = 0.022$ and $P = 0.027$, respectively; Student t test). All tumor models are orthotopic. The asterisks denote a statistically significant difference.

with collagenase incubation in three orthotopic models (Mu89, E0771, and 4T1) and one ectopic model (U87) (Fig. 3 *D* and *E* and Fig. S11).

In contrast to collagen, hyaluronan resists compression. Its negatively charged chains repel because of electrostatic repulsion and trap water, forming a poorly compressible matrix. Consequently, we reasoned that, for storing growth-induced stress, hyaluronan in the compressed tumor interior would be more important than hyaluronan in the tumor periphery, which is under tension. To test this reasoning, we first incubated tumors in hyaluronidase like we did with collagenase. Digesting peripheral hyaluronan had no effect on relaxation. However, when we administered hyaluronidase systemically, we found the tumor relaxation to be reduced in two orthotopic models (Fig. 3*F*). Indeed, hyaluronidase treatment has recently been shown to decompress intratumor vessels (39). Therefore, collagen and hyaluronan store growth-induced stress through their ability to resist tensile and compressive stresses, respectively.

Therapeutic Depletion of CAFs Reduces Solid Stress and Increases Tumor Perfusion. CAFs contribute to the production of collagen, and both of these tumor components contribute to the accumulation of solid stress. Thus, we hypothesized that therapeutic agents that deplete CAFs would alleviate solid stress and decompress vessels. The sonic hedgehog pathway is involved in the generation of the desmoplastic response in pancreatic and other tumors (46). Moreover, depletion of desmoplasia by targeting this pathway in pancreatic tumors combined with gemcitabine has been shown to enhance survival in mice (47). To this end, we inhibited the proliferation of CAFs in highly desmoplastic, hypovascular pancreatic tumors with saridegib (IPI-926), which targets and blocks the smoothened receptor and sonic hedgehog signaling (Fig. 4). Indeed, saridegib treatment reduced growth-induced stress (Fig. 4*C*) and opened compressed vessels (Fig. 4 *A* and *B*). Specifically, saridegib treatment led to a 10% increase in diameter of both blood and lymphatic vessels (Fig. 4*D*) and a 47% increase in the fraction of perfused blood vessels (Fig. 4*E*). One reason that a small change in vessel diameter can lead to a large change in perfused vessel fraction is that decompressing one vessel can reperfuse several downstream vessels. Because the vessel density did not increase significantly (Fig. 4*F*), our work suggests that increased angiogenesis is not required to increase perfusion in hypoperfused tumors. Instead, reducing solid stress can increase the number of functional vessels, and this increase in functional vascular density can lead to increased perfusion, which could enhance drug delivery (48). This mechanism can also explain, in part, the connection between drug delivery and collagen content reported previously by our laboratory (49–52).

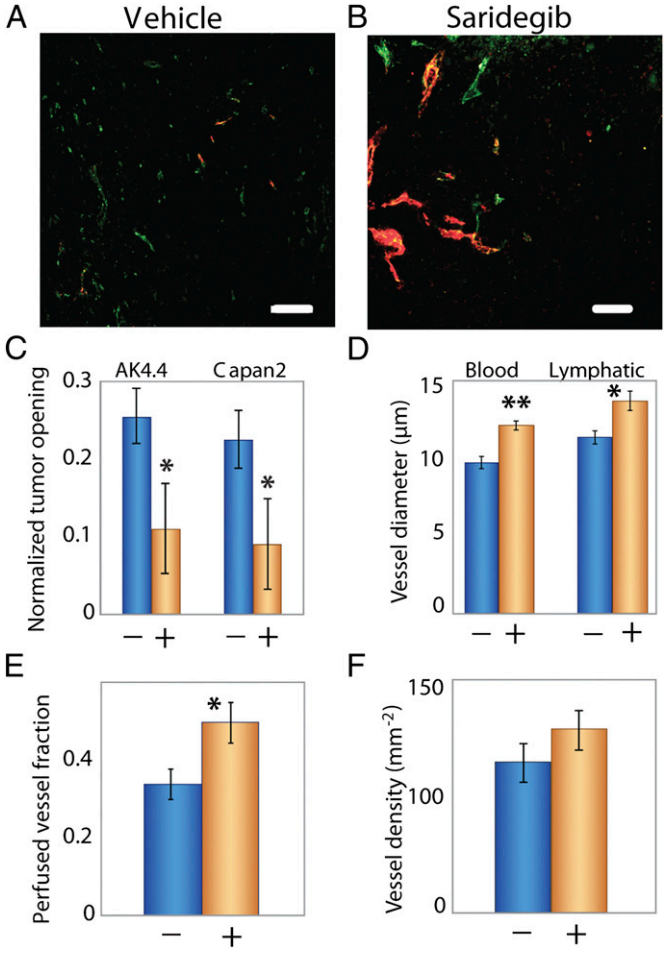

Fig. 4. Saridegib increases tumor vessel diameter and reopens compressed vessels by reducing stress. (*A*) Orthotopically transplanted AK4.4 pancreatic tumors are hypovascular with compressed vessel structures stained with CD31 (green). These tumors also have reduced perfusion, which was detected by lectin (red). (*B*) Treatment with saridegib increased the number of lectin-perfused vessels. (*C*–*F*) Treatment with saridegib reduced stress (*C*; $P = 0.046$ for AK4.4 and $P = 0.022$ for Capan2; Student *t* test) in tumors, leading to increased vessel diameter (*D*; blood vessels: CD31 staining, $P = 0.003$; lymphatic vessels: LYVE-1 staining, $P = 0.004$; Student *t* test) and fraction of perfused vessels (*E*; $P = 0.049$; Student *t* test) without increasing vessel density (*F*; $P =$ not significant) in AK4.4. +, saridegib; −, vehicle. The asterisks denote a statistically significant difference. (Scale bar, 100 μm.)

Discussion

The presence of growth-induced solid stress in tumors had been suspected, but these stresses had to be estimated using theoretical or computational models (30, 34). Here, we presented a simple technique to determine the growth-induced solid stress accumulated within a freshly excised tumor and showed that this stress could be reduced by depleting cancer cells, fibroblasts, collagen, and/or hyaluronan (Fig. 5). Based on our results, solid stress likely develops in two ways in tumors. First, cells generate force during proliferation and contraction. This force is stored as deformations within other cells and the ECM. The matrix is cross-linked to itself in a microstructure, and it links to cells directly through cell matrix and indirectly through cell–cell interactions. Second, because cells within tumors proliferate and create new solid material—cells and matrix fibers—the accumulated material pushes against the surrounding tumor microenvironment. The expansion of the tumor microenvironment is resisted by the surrounding macroenvironment of the normal organ. Because cancer cells proliferate uncontrollably, ignoring contact inhibition signals to stop replicating, their expansion imposes elastic strain on the surrounding tumor microenvironment, storing stress through the deformation of compliant structures and collapsing more fragile structures, such as blood and lymphatic vessels. This solid stress is accumulated within the tumor and maintained even after the tumor is excised. It is this growth-induced or residual solid stress, rather than the stress caused by mechanical interactions with the surrounding macroenvironment of the normal organ, that our technique estimates.

Using this technique, we showed that growth-induced solid stress mediates vessel compression. Compression of vessels by the tumor itself raises an interesting paradox: because tumors need functional blood vessels to supply oxygen and nutrients, why do tumors compress their own vessels? Our hypothesis is that the vessel compression—a hallmark of all solid tumors—could be a mechanism that cancer cells exploit to evade the host's immune response. Immune cells circulate in our body through blood vessels, and thus, vessel compression may reduce their access.

Although many immune cells still infiltrate the tumor, hypoxia and acidity—resulting from impaired perfusion—can attenuate their killing potential (53). Hypoxia also has the potential to convert resident macrophages into protumorigenic cells. In addition, growth factors produced in response to hypoxia (e.g., TGF-β and VEGF) suppress the activity of macrophages and lymphocytes, block the maturation of dendritic cells that process tumor antigens, and present to the immune cells (22). Furthermore, a harsh hypoxic and acidic microenvironment imposes a survival advantage for more malignant cancer cells, harbors the so-called cancer-initiating cells, confers resistance to cell death by apoptosis and autophagy, and enhances the invasive and metastatic potential of cancer cells (54). Finally, hypoxia lowers the efficacy of radiation, chemotherapy, and immunotherapy (22, 55).

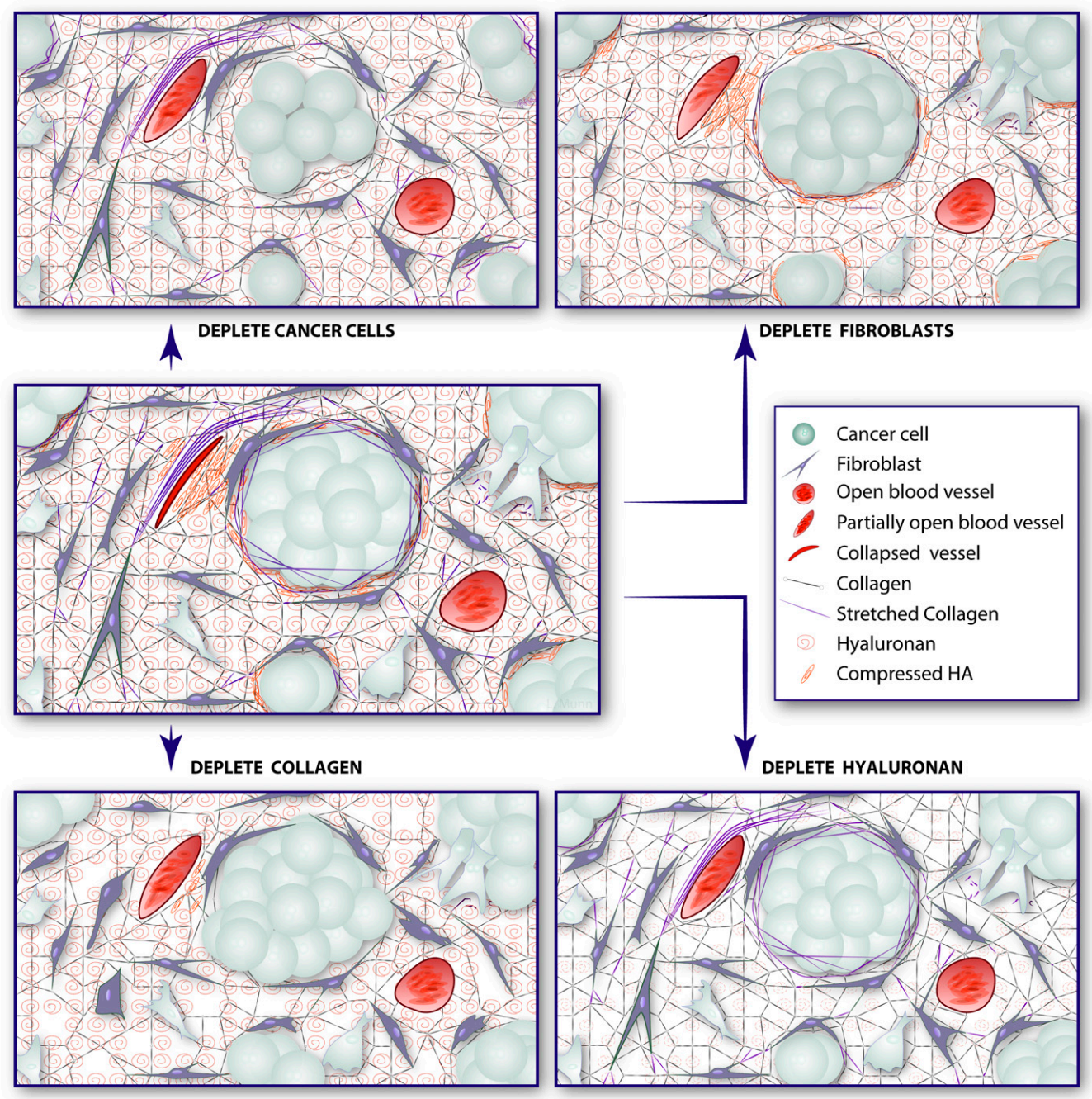

Fig. 5. Strategies to alleviate growth-induced solid stress in tumors. (*Middle*) In an untreated tumor, proliferating cancer cells and activated fibroblasts deform the ECM, resulting in stretched collagen fibers, compressed hyaluronan, and deformed cells—all storing solid stress. This stress compresses intratumor blood and lymphatic vessels. Potential strategies to alleviate solid stress and decompress vessels involve depleting these components. Depleting cancer cells (*Top Left*) or fibroblasts (*Top Right*) relaxes collagen fibers, hyaluronan, and the remaining cells, alleviating solid stress. Depleting collagen (*Bottom Left*) alleviates the stress that was held within these fibers as well as relaxes stretched/activated fibroblasts and compressed cancer cells within nodules. Finally, depleting hyaluronan (*Bottom Right*) alleviates the stored compressive stress, allowing nearby components to decompress. (Note that other stromal cells, such as pericytes, macrophages, and various immune cells that might also control production of collagen or hyaluronan, are not shown to simplify the schematic. Lymphatic vessels are also not shown for the same reason.)

The compression of vessels also creates two potential barriers to drug delivery. First, the collapse of blood vessels hinders access of systemically administered drugs (56). This collapse might explain, in part, the fact that tumors with more ECM might be more resistant to treatment. For instance, pancreatic ductal adenocarcinomas, chondrosarcomas, and chordomas are rich in ECM and refractory to chemotherapy (39, 47, 57). Second, the lack of lymphatic vessel function reduces drainage, leading to uniformly elevated IFP (3, 4). As a result, the transport of large therapeutics, like antibodies and nanoparticles, is reduced, because the dominant mechanism of transport becomes diffusion, which is a very slow process for large particles and macromolecules (58).

It is possible that depleting the ECM to alleviate solid stress and decompress vessels could make it easier for the cancer cells to metastasize by either invading the surrounding tissue or escaping through the blood vessels. Similarly, digesting the matrix to open intratumoral vessels and improve blood flow might promote tumor growth by delivering more nutrients to cancer cells. These concerns need additional study, but several observations suggest that therapies able to ease solid stress and improve perfusion and delivery of drugs counteract any protumor effects (29, 39, 47).

The deformation induced by solid stress is inversely proportional to the tissue stiffness. Indeed, increased tumor tissue stiffness has been linked to tumor incidence and progression (59, 60). Furthermore, the stiffness of the ECM has been shown to direct stem cell differentiation, cell–cell and cell–matrix adhesion, hyaluronan synthesis, and expression of genes that play important roles in invasion and metastasis (60–64). Our technique can be used to determine whether an intervention reduces growth-induced solid stress without measuring the stiffness as long as the experimental group known to be less stiff has a smaller normalized tumor opening. However, to more precisely determine the magnitudes of growth-induced solid stress, measurements of tissue stiffness and growth patterns are necessary.

In conclusion, by developing a simple technique, we showed that it is possible to increase perfusion by alleviating solid stress and thereby, decompressing vessels. It is likely that reducing solid stress would reduce IFP by lowering the venous resistance (9). However, despite this potential to lower IFP, the antisolid stress strategy is distinct from the vessel normalization strategy, which employs direct or indirect antiangiogenic agents to prune immature vessels and fortify the remaining vessels (1, 21). Vessel normalization, in contrast, requires the blood vessels to be open and perfused. This fact explains why antiangiogenic agents have failed thus far in desmoplastic tumors such as pancreatic ductal carcinoma, which has abundant compressed vessels and is hypoperfused. However, the antiangiogenic agents might work if combined judiciously with antisolid stress agents that decompress vessels and improve tumor perfusion. Antisolid stress approaches could also be combined with tumor-targeting ligands (65) and matrix-modifying agents (52) to improve drug delivery and efficacy. The easy to implement, simple technique presented here can rapidly test whether certain tumor components contribute to the accumulation of growth-induced solid stress without the need for measurements of material properties in some cases. Additionally, it can serve as a rapid screen for stress-reducing and perfusion-enhancing drugs.

Materials and Methods

Animal and Tumor Models. Tumors were prepared by implanting a small piece (1 mm^3) of viable tumor tissue from a source tumor animal into the orthotopic site of a male FVB mouse (AK4.4) or a SCID mouse (other cell lines). The orthotopic sites included the mammary fat pad (mfp), pancreas, and flank. Specifically, we used the following 11 cell lines: human melanoma Mu89 (orthotopic flank), human glioblastoma U87 (ectopic flank), human fibrosarcoma HT1080 (orthotopic flank), human colon adenocarcinoma LS174T (ectopic flank), murine melanoma B16F10 (orthotopic flank), murine mammary tumor 4T1 (orthotopic mfp and ectopic flank), murine mammary adenocarcinoma MCaIV (orthotopic mfp and ectopic flank), murine mammary adenocarcinoma E0771 (orthotopic mfp and ectopic flank), murine pancreatic adenocarcinoma Pan02 (orthotopic pancreas), pancreatic adenocarcinoma Capan-2 (orthotopic pancreas), and murine pancreatic adenocarcinoma AK4.4 (orthotopic pancreas). AK4.4 cells were isolated from spontaneous pancreatic tumors arising in $Kras^{G12}$–$p53^{+/-}$ mice (66).

To grow mouse tumors bearing human CAFs, we adopted our previously used procedure (41). Female SCID mice were coimplanted s.c. in the mfp with 5×10^4 E0771 tumor cells and 5×10^5 human CAFs in 0.1 mL PBS (i.e., 1:10 ratio). All animal experiments were done with the approval of the Institutional Animal Care and Use Committee. For each tumor type, 4–12 specimens were used.

Growth-Induced Solid Stress Measurements. When the tumor diameters reached ~1 cm, the animals were anesthetized by injecting 0.2 mL ketamine-xylazine solution (100/10 mg/kg body weight) i.m. Subsequently, each tumor was excised and washed with HBSS, and its three dimensions and weight were measured. To measure the opening, we cut the tumor along its longest axis (~80% of its thickness). Then, the tumor was allowed to relax for 10 min to diminish any transient, poroelastic response. We then measured the opening at the surface of the tumor, in the center, and close to the two edges of the cut. Performing preliminary measurements of the tumor opening, we found that, after 5 min, the opening did not change. Thus, we considered 10 min to be sufficient time for stress relaxation. We report the maximum opening at the center of the tumor. We chose the tumor size to be 1 cm; tumors of smaller size (<0.5 cm) often did not exhibit a measurable opening, whereas larger tumors had large necrotic areas, which affected the measurement. Movies S1 and S2 show the technique performed on a tumor and normal mouse kidney, respectively. Stress was calculated from the measured opening using the mathematical model given in *SI Materials and Methods*.

A description of the IFP measurements, piezoelectric probe measurements, treatments to deplete collagen, hyalouronan, and CAFs, immunostaining methods, and statistical analysis can be found in *SI Materials and Methods*.

ACKNOWLEDGMENTS. We thank Dr. Y. C. Fung and the late Dr. R. Skalak for inspiring us to work on the residual stresses in tumors, Dr. C. Fernandez-Del Castillo for his help with the pancreatic tumor studies, Dr. P. Alford for assistance with the implementation of the mathematical model, Drs. J. Baish, A. Grodzinsky, P. Netti, and T. Padera, and various members of the Steele Laboratory for helpful input, and Sylvie Roberge, Julia Kahn, and Carolyn Smith for outstanding technical assistance. We thank Infinity Pharmaceuticals for providing saridegib. T.S. was supported by FP7 Marie-Curie IRG Grant PIRG08-GA-2010-276894. This work was supported by National Institutes of Health Grants P01CA080124 and R01CA126642 and Department of Defense Breast Cancer Research Innovator Award W81XWH-10-1-0016 (to R.K.J.).

1. Jain RK (2005) Normalization of tumor vasculature: An emerging concept in antiangiogenic therapy. *Science* 307:58–62.
2. Young JS, Lumsden CE, Stalker AL (1950) The significance of the tissue pressure of normal testicular and of neoplastic (Brown-Pearce carcinoma) tissue in the rabbit. *J Pathol Bacteriol* 62:313–333.
3. Jain RK, Baxter LT (1988) Mechanisms of heterogeneous distribution of monoclonal antibodies and other macromolecules in tumors: Significance of elevated interstitial pressure. *Cancer Res* 48:7022–7032.
4. Baxter LT, Jain RK (1989) Transport of fluid and macromolecules in tumors. I. Role of interstitial pressure and convection. *Microvasc Res* 37:77–104.
5. Boucher Y, Baxter LT, Jain RK (1990) Interstitial pressure gradients in tissue-isolated and subcutaneous tumors: Implications for therapy. *Cancer Res* 50:4478–4484.
6. Boucher Y, Kirkwood JM, Opacic D, Desantis M, Jain RK (1991) Interstitial hypertension in superficial metastatic melanomas in humans. *Cancer Res* 51:6691–6694.
7. Roh HD, et al. (1991) Interstitial hypertension in carcinoma of uterine cervix in patients: Possible correlation with tumor oxygenation and radiation response. *Cancer Res* 51:6695–6698.
8. Less JR, et al. (1992) Interstitial hypertension in human breast and colorectal tumors. *Cancer Res* 52:6371–6374.
9. Boucher Y, Jain RK (1992) Microvascular pressure is the principal driving force for interstitial hypertension in solid tumors: Implications for vascular collapse. *Cancer Res* 52:5110–5114.
10. Gutmann R, et al. (1992) Interstitial hypertension in head and neck tumors in patients: Correlation with tumor size. *Cancer Res* 52:1993–1995.
11. Boucher Y, Lee I, Jain RK (1995) Lack of general correlation between interstitial fluid pressure and oxygen partial pressure in solid tumors. *Microvasc Res* 50:175–182.
12. Boucher Y, Leunig M, Jain RK (1996) Tumor angiogenesis and interstitial hypertension. *Cancer Res* 56:4264–4266.

13. Padera TP, et al. (2002) Lymphatic metastasis in the absence of functional intratumor lymphatics. *Science* 296:1883–1886.
14. Tong RT, et al. (2004) Vascular normalization by vascular endothelial growth factor receptor 2 blockade induces a pressure gradient across the vasculature and improves drug penetration in tumors. *Cancer Res* 64:3731–3736.
15. Jain RK, Tong RT, Munn LL (2007) Effect of vascular normalization by antiangiogenic therapy on interstitial hypertension, peritumor edema, and lymphatic metastasis: Insights from a mathematical model. *Cancer Res* 67:2729–2735.
16. Hobbs SK, et al. (1998) Regulation of transport pathways in tumor vessels: Role of tumor type and microenvironment. *Proc Natl Acad Sci USA* 95:4607–4612.
17. Griffon-Etienne G, Boucher Y, Brekken C, Suit HD, Jain RK (1999) Taxane-induced apoptosis decompresses blood vessels and lowers interstitial fluid pressure in solid tumors: Clinical implications. *Cancer Res* 59:3776–3782.
18. Padera TP, et al. (2004) Pathology: Cancer cells compress intratumour vessels. *Nature* 427:695.
19. Netti PA, Roberge S, Boucher Y, Baxter LT, Jain RK (1996) Effect of transvascular fluid exchange on pressure-flow relationship in tumors: A proposed mechanism for tumor blood flow heterogeneity. *Microvasc Res* 52:27–46.
20. Baish JW, Netti PA, Jain RK (1997) Transmural coupling of fluid flow in microcirculatory network and interstitium in tumors. *Microvasc Res* 53:128–141.
21. Jain RK (2001) Normalizing tumor vasculature with anti-angiogenic therapy: A new paradigm for combination therapy. *Nat Med* 7:987–989.
22. Goel S, et al. (2011) Normalization of the vasculature for treatment of cancer and other diseases. *Physiol Rev* 91:1071–1121.
23. Winkler F, et al. (2004) Kinetics of vascular normalization by VEGFR2 blockade governs brain tumor response to radiation: Role of oxygenation, angiopoietin-1, and matrix metalloproteinases. *Cancer Cell* 6:553–563.
24. Batchelor TT, et al. (2007) AZD2171, a pan-VEGF receptor tyrosine kinase inhibitor, normalizes tumor vasculature and alleviates edema in glioblastoma patients. *Cancer Cell* 11:83–95.
25. Willett CG, et al. (2009) Efficacy, safety, and biomarkers of neoadjuvant bevacizumab, radiation therapy, and fluorouracil in rectal cancer: A multidisciplinary phase II study. *J Clin Oncol* 27:3020–3026.
26. Carmeliet P, Jain RK (2011) Principles and mechanisms of vessel normalization for cancer and other angiogenic diseases. *Nat Rev Drug Discov* 10:417–427.
27. Chauhan VP, et al. (2012) Normalization of tumour blood vessels improves the delivery of nanomedicines in a size-dependent manner. *Nat Nanotechnol* 7:383–388.
28. Sorensen AG, et al. (2009) A "vascular normalization index" as potential mechanistic biomarker to predict survival after a single dose of cediranib in recurrent glioblastoma patients. *Cancer Res* 69:5296–5300.
29. Sorensen AG, et al. (2012) Increased survival of glioblastoma patients who respond to antiangiogenic therapy with elevated blood perfusion. *Cancer Res* 72:402–407.
30. Skalak R, Zargaryan S, Jain RK, Netti PA, Hoger A (1996) Compatibility and the genesis of residual stress by volumetric growth. *J Math Biol* 34:889–914.
31. Helmlinger G, Netti PA, Lichtenbeld HC, Melder RJ, Jain RK (1997) Solid stress inhibits the growth of multicellular tumor spheroids. *Nat Biotechnol* 15:778–783.
32. Cheng G, Tse J, Jain RK, Munn LL (2009) Micro-environmental mechanical stress controls tumor spheroid size and morphology by suppressing proliferation and inducing apoptosis in cancer cells. *PLoS One* 4:e4632.
33. Tse JM, et al. (2012) Mechanical compression drives cancer cells toward invasive phenotype. *Proc Natl Acad Sci USA* 109:911–916.
34. Roose T, Netti PA, Munn LL, Boucher Y, Jain RK (2003) Solid stress generated by spheroid growth estimated using a linear poroelasticity model small star, filled. *Microvasc Res* 66:204–212.
35. Chuong CJ, Fung YC (1986) On residual stresses in arteries. *J Biomech Eng* 108: 189–192.
36. Omens JH, Vaplon SM, Fazeli B, McCulloch AD (1998) Left ventricular geometric remodeling and residual stress in the rat heart. *J Biomech Eng* 120:715–719.
37. Xu G, Bayly PV, Taber LA (2009) Residual stress in the adult mouse brain. *Biomech Model Mechanobiol* 8:253–262.
38. Sarntinoranont M, Rooney F, Ferrari M (2003) Interstitial stress and fluid pressure within a growing tumor. *Ann Biomed Eng* 31:327–335.
39. Provenzano PP, et al. (2012) Enzymatic targeting of the stroma ablates physical barriers to treatment of pancreatic ductal adenocarcinoma. *Cancer Cell* 21:418–429.
40. Perentes JY, et al. (2009) In vivo imaging of extracellular matrix remodeling by tumor-associated fibroblasts. *Nat Methods* 6:143–145.
41. Duda DG, et al. (2010) Malignant cells facilitate lung metastasis by bringing their own soil. *Proc Natl Acad Sci USA* 107:21677–21682.
42. Nagy JA, et al. (1989) Pathogenesis of tumor stroma generation: A critical role for leaky blood vessels and fibrin deposition. *Biochim Biophys Acta* 948:305–326.
43. Dvorak HF (2003) Rous-Whipple Award Lecture. How tumors make bad blood vessels and stroma. *Am J Pathol* 162:1747–1757.
44. Kalluri R, Zeisberg M (2006) Fibroblasts in cancer. *Nat Rev Cancer* 6:392–401.
45. Sander EA, Stylianopoulos T, Tranquillo RT, Barocas VH (2009) Image-based biomechanics of collagen-based tissue equivalents. *IEEE Eng Med Biol Mag* 28:10–18.
46. Bailey JM, et al. (2008) Sonic hedgehog promotes desmoplasia in pancreatic cancer. *Clin Cancer Res* 14:5995–6004.
47. Olive KP, et al. (2009) Inhibition of Hedgehog signaling enhances delivery of chemotherapy in a mouse model of pancreatic cancer. *Science* 324:1457–1461.
48. Baish JW, et al. (2011) Scaling rules for diffusive drug delivery in tumor and normal tissues. *Proc Natl Acad Sci USA* 108:1799–1803.
49. Netti PA, Berk DA, Swartz MA, Grodzinsky AJ, Jain RK (2000) Role of extracellular matrix assembly in interstitial transport in solid tumors. *Cancer Res* 60:2497–2503.
50. Brown E, et al. (2003) Dynamic imaging of collagen and its modulation in tumors in vivo using second-harmonic generation. *Nat Med* 9:796–800.
51. McKee TD, et al. (2006) Degradation of fibrillar collagen in a human melanoma xenograft improves the efficacy of an oncolytic herpes simplex virus vector. *Cancer Res* 66:2509–2513.
52. Diop-Frimpong B, Chauhan VP, Krane S, Boucher Y, Jain RK (2011) Losartan inhibits collagen I synthesis and improves the distribution and efficacy of nanotherapeutics in tumors. *Proc Natl Acad Sci USA* 108:2909–2914.
53. Facciabene A, et al. (2011) Tumour hypoxia promotes tolerance and angiogenesis via CCL28 and T(reg) cells. *Nature* 475:226–230.
54. Wilson WR, Hay MP (2011) Targeting hypoxia in cancer therapy. *Nat Rev Cancer* 11: 393–410.
55. Carmeliet P, Jain RK (2011) Molecular mechanisms and clinical applications of angiogenesis. *Nature* 473:298–307.
56. Jain RK (1988) Determinants of tumor blood flow: A review. *Cancer Res* 48: 2641–2658.
57. D'Adamo DR (2011) Appraising the current role of chemotherapy for the treatment of sarcoma. *Semin Oncol* 38(Suppl 3):S19–S29.
58. Jain RK, Stylianopoulos T (2010) Delivering nanomedicine to solid tumors. *Nat Rev Clin Oncol* 7:653–664.
59. Levental KR, et al. (2009) Matrix crosslinking forces tumor progression by enhancing integrin signaling. *Cell* 139:891–906.
60. Goetz JG, et al. (2011) Biomechanical remodeling of the microenvironment by stromal caveolin-1 favors tumor invasion and metastasis. *Cell* 146:148–163.
61. Koike C, et al. (2002) Solid stress facilitates spheroid formation: Potential involvement of hyaluronan. *Br J Cancer* 86:947–953.
62. Engler AJ, Sen S, Sweeney HL, Discher DE (2006) Matrix elasticity directs stem cell lineage specification. *Cell* 126:677–689.
63. Demou ZN (2010) Gene expression profiles in 3D tumor analogs indicate compressive strain differentially enhances metastatic potential. *Ann Biomed Eng* 38:3509–3520.
64. Reinhart-King CA (2011) How matrix properties control the self-assembly and maintenance of tissues. *Ann Biomed Eng* 39:1849–1856.
65. Sugahara KN, et al. (2010) Coadministration of a tumor-penetrating peptide enhances the efficacy of cancer drugs. *Science* 328:1031–1035.
66. Hingorani SR, et al. (2005) Trp53R172H and KrasG12D cooperate to promote chromosomal instability and widely metastatic pancreatic ductal adenocarcinoma in mice. *Cancer Cell* 7:469–483.